JOURNAL OF SOLID STATE CHEMISTRY 107, 201–210 (1993)

Study on the Internal Action and Existent State of ZrO_2 in Fused Iron Catalysts of Different Compositions

WANG WEN-XIANG,* LIU ZHENG,† AND LI FAN*

*Department of Chemistry, Zhengzhou University, Zhengzhou, People's Republic of China; and †Chemical Engineering Department, Zhengzhou Light Industry Institute, Zhengzhou, Henan, People's Republic of China

Received August 14, 1992; in revised form March 1, 1993; accepted March 3, 1993

By use of XRD, we have found that cubic crystals $Ca_xZr_{1-x}O_{2-x}$(CaF_2 structure) exist in the fused iron catalyst containing ZrO_2 and a small amount of CaO. We also found that Fe^{2+} could enter monoclinic ZrO_2 lattices to convert it into cubic $ZrO_2(Fe_xZr_{1-x}O_{2-x})$, which in turn causes a small portion of Fe_3O_4 to be broken down to form Fe_2O_3(10R). SEM observation of the catalyst surface indicates that $Ca_xZr_{1-x}O_{2-x}$ separates out of the α-Fe lattice and is concentrated in the cracks or channels of the reduced catalyst, while in the unreduced catalyst, $Ca_xZr_{1-x}O_{2-x}$ has a relatively uniform dispersion. For the catalyst without CaO, however, ZrO_2 exhibits an even distribution on the surface of both reduced and unreduced catalysts. The result of the specific surface area measurement shows that the BET surface area of the catalyst decreases somewhat as the content of ZrO_2 increases. By the thermoanalytical technique (TG), we have further confirmed that ZrO_2 promotes the reduction of the fused iron catalyst. If ZrO_2 and CaO are added together to the catalyst the reduction behavior of the catalyst is greatly improved.

Introduction

Early in 1958, Blumenthal showed that zirconium dioxide can serve as a catalyst or catalyst promoter in a wide variety of organic reactions (1). Recently, Ichikawa (2) reported that there is a higher selectivity of ethanol over Rh/ZrO_2. Several papers (3–6) stated that coprecipitated catalysts with ZrO_2 as support and promoter exhibit high activity and selectivity for methanol formation from $CO_2 + H_2$.

A report from Oppau in Ref. (7) describes a detailed study of fused iron oxide catalysts for hydrogenation of carbon monoxide. It is stated that the acidic components, SiO_2, TiO_2, and ZrO_2, promoted formation of alcohols and that ZrO_2 was the most effective. Kagan (8) reported that an optimum content of ZrO_2 in fused iron catalysts for alcohols from $CO + H_2$ could improve stability, activity, and selectivity of catalysts. Recently, in our laboratory (9), a study of alcohol synthesis from $CO + H_2$ over a triply promoted fused iron catalyst doped with different metal oxides showed that the catalyst containing ZrO_2 provides the highest yield of alcohols. Evidently, ZrO_2 is also a good promoter for alcohol synthesis over fused iron catalysts.

It is well-known that ZrO_2 has three different crystal forms, monoclinic, tegragonal, and cubic; only monoclinic ZrO_2 is stable at room temperature. Maskell and Stelle (12) indicated that cubic ZrO_2 can be stabilized at room temperature by addition of divalent oxides, and that cubic ZrO_2 contains oxygen anionic vacancies at high concentrations. Jackson and Ekerdt (10) suggested that the active site for CO hydrogenation over ZrO_2 was an oxygen anion vacancy. Silver *et al.*, in their study (11), support the hypothesis that the active site for CO hydrogenation over ZrO_2 is an oxygen anion vacancy.

0022-4596/93 $5.00

TABLE I

CHARACTERISTICS OF SAMPLES

Sample symbol[a]	Promoter content (wt%)				Shape	Fe^{2+}/Fe^{3+}
	ZrO_2	Al_2O_3	K_2O	CaO		
$A_{110\text{-}5Q}$	—	2	1	1	Sphere	0.66
$Z_1A_1K_1C_1F$	1	1	1	1	Sphere	0.57
$Z_2A_1K_1C_1F$	2	1	1	1	Irregular	0.58
$Z_4A_1K_1C_1F$	4	1	1	1	Irregular	0.57
$Z_4A_2K_1C_1F$	4	2	1	1	Irregular	0.53
Z_4F	4				Irregular	0.53
Z_4K_1F	4		1		Irregular	0.52
Z_4C_1F	4			1	Irregular	0.37
$Z_{11}F$	11				Irregular	0.41

[a] $Z = ZrO_2$, $A = Al_2O_3$, $K = K_2O$, $C = CaO$, and $F = FeO_x$ (i.e., iron oxides, as the balance of wt%).

Therefore, to understand the role of ZrO_2 as promoter, it is necessary to carry out a further study of the structure of ZrO_2 in catalysis. This paper aims to investigate the state of ZrO_2 on fused iron catalysts at different compositions, and the surface characteristics. The internal action of ZrO_2 with iron oxides and other promoters including CaO, K_2O, and Al_2O_3 is also a problem of great interest.

Experimental

1. Sample Preparation

(*a*) *Catalysts.* Fused iron catalysts were prepared by mixing appropriate proportions of ZrO_2, KNO_3, $CaCO_3$, and Al_2O_3 with Fe_3O_4 and fusing them at about 1600°C to generate promoters that are as evenly dispersed in Fe_3O_4 as possible, and then rapidly cooling the mixture. The concentration of promoters (wt%) and characteristics of catalyst samples are summarized in Table I. Concerning the notation: $Z_2A_1K_1C_1F$, for example, denotes ZrO_2 2%, Al_2O_3 1%, K_2O 1%, and CaO 1% in weight, respectively, the rest being iron oxides, FeO_x.

(*b*) *Sample* ZrO_2^*. The sample $Z_4A_1K_1C_1F$ was soaked in concentrated hydrochloric acid. The undissolved material was filtered and washed to get rid of Cl^-. The white crystal obtained was ZrO_2^*.

(*c*) *Sample ZC.* This sample was prepared by calcining the mixture of 5 wt% CaO and 95 wt% ZrO_2 (monoclinic) for 4 h at 1300°C.

For prereduced samples ($Z_4A_1K_1C_1F$, Z_4F), purified H_2 was passed through a tubular reactor where the sample was inside. The temperature was raised from room temperature to 475°C in 2 h, maintained for 5 h, then raised to 500°C in 1 h and maintained there for 16 h so that iron oxide was reduced. Afterward, the catalyst was cooled while the reducing gas (H_2) was continuously passed through the reactor until the temperature was lowered to room temperature. To passivate the reduced catalyst, N_2 containing a small amount of O_2 was allowed to flow into the reactor until a thin layer of oxides formed on the catalyst surface, so that the catalyst was not oxidized (burnt) in air.

2. Sample Characterization

(*a*) X-ray diffraction (XRD) powder patterns were obtained with a Rigaku D/MAX-3B X-ray diffractometer at room temperature; the radiation used was Cu K_α (λ = 1.5418 Å) at angles (2θ) of 80° to 20° and a voltage/current settings 40 kV, 20 mA.

(*b*) *Scanning electron microscope (SEM)*

observation. The crushed unreduced catalysts were coated with carbon. The prereduced catalysts were placed onto the lighted-surface grain as the sample. Care was taken that the samples would not be polluted and damaged. The SEM photograph was obtained by using a KYKY-AMRAY-1000B scanning electron microscope. An elemental analysis was carried out by KYKY-AMRAY-1000B/TN-5400 energy dispersive X-ray (EDX) analyzer.

(*c*) *Determination of specific surface area*. The prereduced samples were reduced again in situ by passing hydrogen through with a space velocity of about 25,000 h^{-1}. The reduction temperature was maintained at 480°C for 1 h and at 500°C for 2 h. The measurement of BET surface area was carried out by N_2 adsorption, with the continuous flow method, using a modified gas-chromatographic instrument at liquid-N_2 temperature. Hydrogen was used as the carrier gas. The BET surface area of the reduced catalysts was calculated by the appropriate multilayer adsorption theory.

(*d*) *Reduction experiment*. The reduction was conducted by using a Japan Rigaku TG-DTA-thermoanalyzer. The sample (TG < 50 mg, 300 mesh) was exposed to 60 ml/min purified H_2, heated to 200°C, and maintained for 30 min, and afterward, heated to 525°C at a constant rate, 5°C/min. The reduction characteristics of samples are listed in Table V. The reduction rate (v) is represented in terms of $d\alpha/dt$, where α is the reduction degree and t is the time.

Results and Discussion

1. XRD Analysis

(*a*) *The state of ZrO_2 on unreduced catalysts*. Figure 1 shows the XRD pattern of $Z_1A_1K_1C_1F$, $Z_4A_2K_1C_1F$, ZrO_2^*, and *ZC*. Undoubtedly, the chief XRD peaks for the fused iron catalyst belong to Fe_3O_4(56F) (*13*). There is only 1 wt% ZrO_2 in $Z_1A_1K_1C_1F$; no other particular XRD peaks except Fe_3O_4(56F) are present in $Z_1A_1K_1C_1F$.

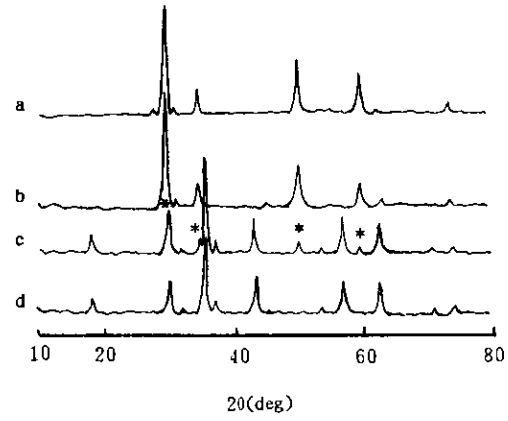

FIG. 1. X-ray diffraction patterns of samples (a) *ZC*, (b) ZrO_2^*, (c) $Z_4A_1K_1C_1F$, and (d) $Z_1A_1K_1C_1F$.

Special XRD peaks appear with an increase of ZrO_2 in the catalyst, as shown by asterisk (*); the values have been summarized in Table II. From Table II it can be seen that the d (Å) values of some * peaks in Fig. 1c coincide with those of the principal XRD peaks of $Ca_{0.15}Zr_{0.85}O_{1.85}$, as shown in Table II, which indicate that $Ca_{0.15}Zr_{0.85}O_{1.85}$ (molar ratio of Ca : Zr : O being 0.15 : 0.85 : 1.85) possibly exists in $Z_4A_1K_1C_1F$.

In order to further verify the existence of ZrO_2 in the catalyst, we have carried out an XRD on *ZC* and ZrO_2^*. The test result shows that the d values of XRD peaks of *ZC* and ZrO_2^* basically coincide with those of $Ca_{0.15}Zr_{0.85}O_{1.85}$, and the main XRD peaks corresponds to the asterisk (*) peaks of $Z_4A_1K_1C_1F$. This can be seen clearly in Fig. 1. From Table II it is found that d values of the XRD peaks of *ZC*, ZrO_2^* deviate slightly from those of the face centered cubic crystal ZrO_2(12F). It has been reported in literature (*14*) that pure face-centered cubic crystal ZrO_2(12F) only exists at temperatures above 1900°C. To stabilize cubic crystal ZrO_2 at room temperature, one must add a small amount of alkali earth metal ions to the lattice of ZrO_2. This kind of cubic crystal possesses the CaF_2 structure. In practice, the temperature never reaches 1900°C; the XRD peaks of cubic crystal ZrO_2 in the samples

TABLE II

XRD DATA OF * PEAKS ON FIG. 1c, FIG. 2, AND FIG. 3

$Ca_{0.15}Zr_{0.85}O_{1.85}$ from JCPDS		ZrO_2(12F) from JCPDS		ZrO_2^*		*ZC*	
I/I_0	d (Å)	I/I_0	d (Å)	I/I_0	d (Å)	I/I_0	d (Å)
100	2.96	100	2.933	100	2.967	100	2.968
45	1.82	50	1.802	37	1.816	43	1.816
25	1.55	25	2.551	22	2.569	23	2.57
20	2.56	20	1.534	18	1.55	33	1.55
6	1.18	5	1.471	7	2.883	7	3.169
5	1.05	5	1.271	5	1.536	5	2.850
4	1.481	5	1.167	5	1.483	6	1.482
4	1.248	5	1.41	3	1.284	5	1.178
4	1.148			6	1.178	17	1.544
				4	1.146	7	1.283

$Z_4A_1K_1C_1F$		Z_4C_1F		$Z_{11}F$		Z_4F		Z_4K_1F	
I/I_0	d (Å)	I/I_0	d (Å)	I/I_0	d (Å)	I/I_0	d (Å)	I/I_0	d (Å)
32	2.972	5	2.960	5	2.954	5	2.94	9	2.953
3	1.812	3	1.809	2	1.799	3	1.807	2	1.799
2	2.57	2	2.56	1	2.56	2	2.56	1	2.56
2	1.55	2	1.53	1	1.533	2	1.53	1	1.53

are caused by the added CaO, and Ca^{2+} dissolved in ZrO_2 really stabilizes the cubic crystal. The CaO-stabilized zirconia has the formula (*20*) $Ca_xZr_{1-x}O_{2-x}$ ($0.1 \lesssim x \lesssim 0.2$). We believe that ZrO_2^* and *ZC* exist in the form of $Ca_xZr_{1-x}O_{2-x}$, because Ca^{2+} entering the ZrO_2 lattice gives rise to XRD peaks in $Ca_xZr_{1-x}O_{2-x}$ that slightly deviate from those of pure ZrO_2(12F). In the catalyst, ZrO_2 should exist in the form of a CaF_2-type of cubic crystal $Ca_xZr_{1-x}O_{2-x}$ ($0.1 \lesssim x \lesssim 0.2$).

Figures 2 and 3 show XRD patterns of catalysts Z_4K_1F, Z_4C_1F, Z_4F, and $Z_{11}F$; the

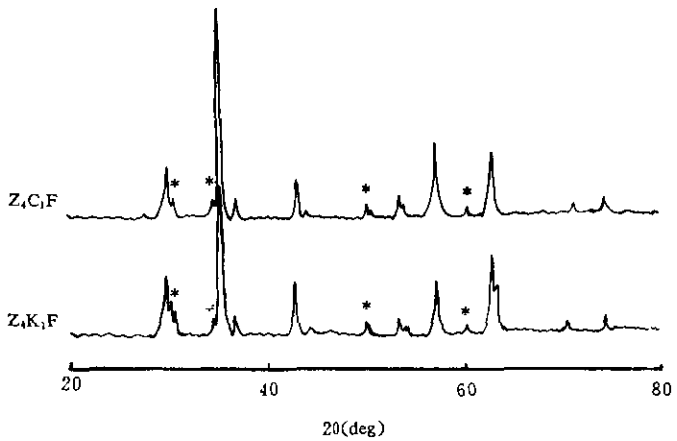

FIG. 2. X-ray diffraction patterns of samples.

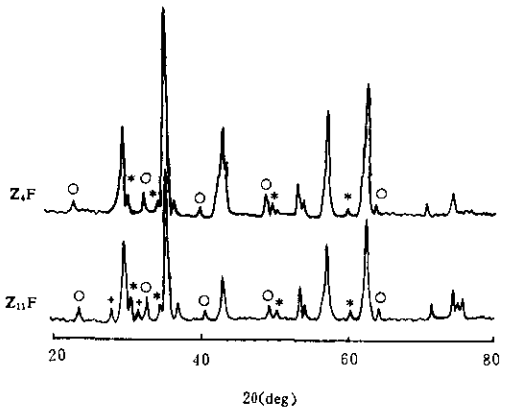

FIG. 3. X-ray diffraction patterns of samples.

d values of asterisk (*) peaks and their relative intensity are shown in Table II. From Table II it is found that *d* values of * peaks are roughly the same as those of the strong peaks of cubic ZrO_2(12F), which shows that the ZrO_2 in $Z_{11}F$, Z_4F, Z_4K_1F, and Z_4C_1F probably is a cubic crystal. The cubic crystal ZrO_2 in Z_4C_1F is stabilized by CaO, but it is not clear why cubic ZrO_2 exists in Z_4K_1F, Z_4F, and $Z_{11}F$. We believe that this situation may result from Fe^{2+}, because the mean ion radius of Fe^{2+} (0.76 Å) is roughly equal to and smaller than that of Ca^{2+} (1.14 Å), and the electric charge of Fe^{2+} is also equal to that of Ca^{2+}. Like Ca^{2+}, Fe^{2+} may enter the crystal lattice of ZrO_2 and render the initially monoclinic ZrO_2 stable as a cubic crystal in the form $Fe_x^{2+}Zr_{1-x}O_{2-x}$ ($x < 1$).

It can be seen in Fig. 3 that there are special XRD peaks (marked in signs + and ○), the *d* values of which have been listed in Table III. Comparing the *d* values of the ○ peaks with those of Fe_2O_3(10R) we find that there exists a trigonal configuration of Fe_2O_3(10R). The presence of Fe_2O_3(10R) in Z_4F and $Z_{11}F$ may be related to the fact that a part of Fe^{2+} enter the ZrO_2 lattice, which causes a small portion of Fe_3O_4 to be broken down and to form Fe_2O_3(10R). The Fe_2O_3(10R) phase, however, is rarely present in samples containing K_2O and CaO. This may be due to the fact that the reaction of K_2O and CaO with Fe_2O_3(10R) leads to the formation of ferrites (*15*, *16*). Comparing the *d* values of + peaks with those of standard ZrO_2 (monoclinic), we can be certain that monoclinic ZrO_2 exists in $Z_{11}F$, but it is not found in Z_4F. This may be due to the fact that the ZrO_2 content in $Z_{11}F$ is much greater than that in Z_4F; the Fe^{2+}/Fe^{3+} (atomic ratio) of $Z_{11}F$ is smaller than that of Z_4F, and the chance of Fe^{2+} entering ZrO_2 lattice is smaller. From the above analysis, it is found that in the process of the sample preparation, Fe^{2+} possibly enters lattices of ZrO_2 and converts it into a stable cubic crystal, which exists in the form of $Fe_x^{2+}Zr_{1-x}O_{2-x}$ ($x < 1$, 12F); meanwhile, Fe_3O_4

TABLE III

XRD DATA OF ○, + PEAKS ON FIG. 3

Monoclinic ZrO_2 from JCPDS		Fe_2O_3(10R) from JCPDS		$Z_{11}F$		Z_4F	
I/I_0	*d* (Å)	I/I_0	*d* (Å)	I/I_0	*d* (Å)	I/I_0	*d* (Å)
100	3.16	100	2.703	10	○2.207	11	○2.707
65	2.834	70	2.519	100	2.53	100	2.53
20	2.617	36	1.696	3	○1.697	6	○1.699
18	3.69	33	3.69	4	○3.69	5	○3.69
14	3.63	22	1.487	2	○1.456	4	○1.841
12	1.82	21	1.45	3	○2.214	4	○1.456
10	1.541	17	2.208	4	○1.845	2	○2.209
18	1.845	31	1.84	7	+3.169		
				4	+2.842		

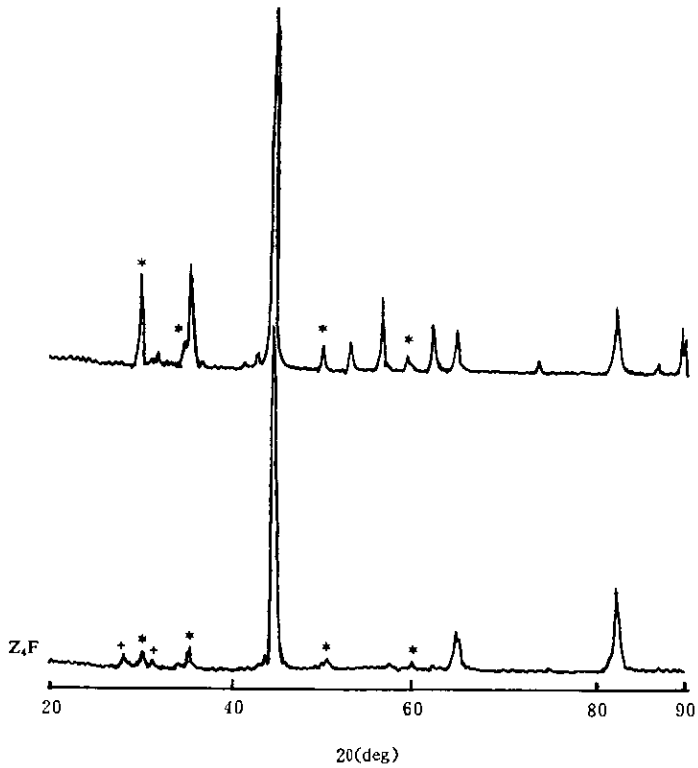

FIG. 4. X-ray diffraction patterns of reduced samples.

partly breaks down to form a new phase Fe_2O_3(10R). If Fe^{2+} enters the lattice of ZrO_2, the Fe^{2+}, after reduction, will get dispersed and not be easily sinterable.

On the basis of relative strength of metal–oxygen bonds, the order of decreasing acid strength is TiO_2, Al_2O_3, ThO_2, BeO, then ZrO_2 (*17*). Thus, when ZrO_2 is heated with a strong base such as K_2O, a metazirconate is formed. Potassium zirconate has been detected by FTIR in the fused iron catalyst containing K_2O and ZrO_2 (*18*). Nevertheless, the potassium zirconate cannot be detected in the presence of Al_2O_3, due to the reaction of Al_2O_3 with K_2O in preference to ZrO_2. At present, no compounds of Al_2O_3 and ZrO_2 are known.

(*b*) *The existence of ZrO_2 in reduced catalysts.* Figure 4 shows XRD patterns of the reduced $Z_4A_1K_1C_1F$ and Z_4F. Several main XRD peaks are associated with α-Fe, as identified by comparison with JCPDS cards. The *d* values of the * peaks of $Z_4A_1K_1C_1F$ are 2.9646, 1.815, 2.56, and 1.546. As we have verified earlier, these peaks are the strongest among those produced by cubic $Ca_xZr_{1-x}O_{2-x}$. Thus we can conclude that with respect to the reduced state of catalyst $Z_4A_1K_1C_1F$, ZrO_2 still exists in the form of cubic $Ca_xZr_{1-x}O_{2-x}$ ($0.1 \leq x \leq 0.2$, CaF_2 structure).

On comparing the *d* values (2.96, 1.797, 2.56, and 1.53) of the asterisk (*) peaks in Z_4F and the *d* values (3.16 and 2.84) of the ○ peaks shown in Fig. 4 with those of ZrO_2(12F), shown in Table II, and with those of ZrO_2 (monoclinic), shown in Table III, respectively, we see that in addition to cubic crystal ZrO_2(12F), a small portion of monoclinic ZrO_2 exists in the reduced Z_4F, while no such ZrO_2 exists in the unreduced Z_4F. This suggests that if Fe^{2+} enters ZrO_2 lattices and stabilizes the cubic crystal, Fe^{2+} will be eliminated (changed to α-Fe) after it

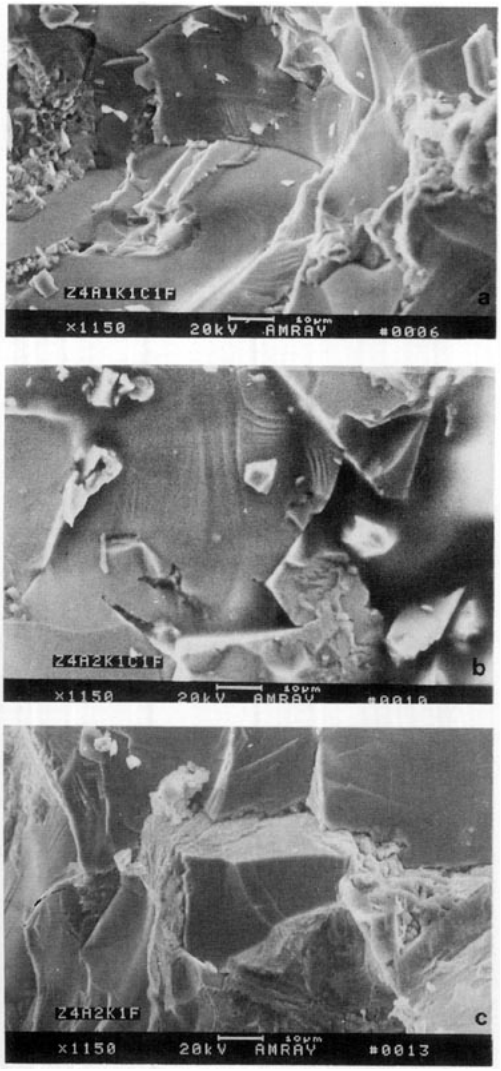

FIG. 5. SEM photographs of unreduced catalyst.

is reduced, a small portion of cubic ZrO_2 being converted into monoclinic ZrO_2. This, in turn, also provides experimental evidence for Fe^{2+} entering the ZrO_2 lattice.

2. *SEM Analysis*

(*a*) *The SEM of the unreduced catalysts.* Figure 5 shows the scanning electron micrographs of the interface of the crushed catalysts $Z_4A_1K_1C_1F$, $Z_4A_2K_1C_1F$, and $Z_4A_2K_1F$. No significant difference is seen among them, which seem to be built of bricks. For $Z_4A_2K_1F$, however, the interfacial structure piled up by bricks is relatively more regular, and the size of the particle is also smaller than that of $Z_4A_1K_1C_1F$ and $Z_4A_2K_1C_1F$. The result of elemental analysis indicates that the distribution of ZrO_2 is relatively even in the unreduced fused iron catalyst and that no highly concentrated regions of ZrO_2 exists in these catalysts.

(*b*) *The SEM of the reduced catalysts.* Figure 6 shows the SEM photographs of the

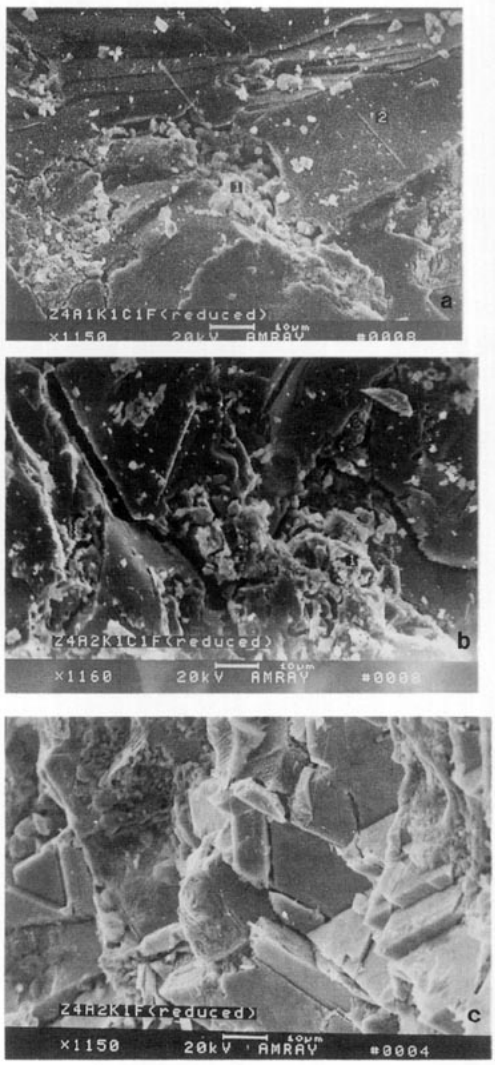

FIG. 6. SEM photographs of reduced catalyst.

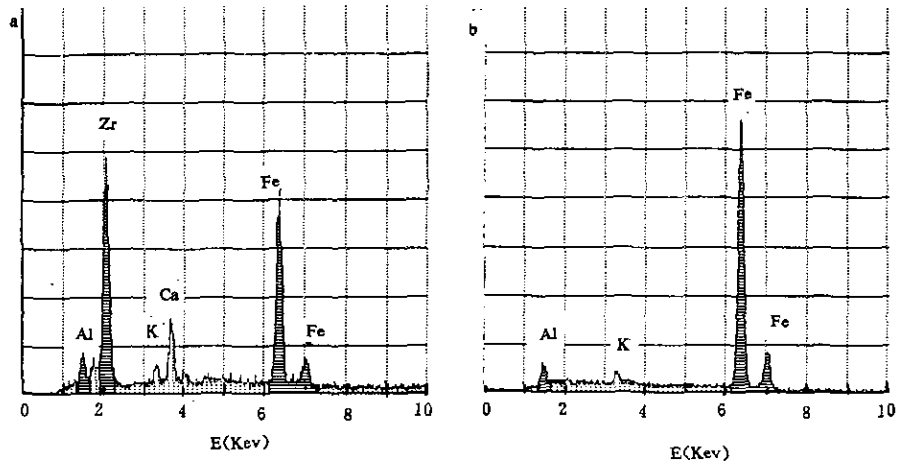

FIG. 7. Energy dispersion X-ray spectrum of the reduced $Z_4A_1K_1C_1F$ (a) point 1 and (b) point 2.

reduced catalysts $Z_4A_1K_1C_1F$, $Z_4A_2K_1C_1F$, and $Z_4A_2K_1F$. It can be seen that the interfaces of $Z_4A_2K_1C_1F$ and $Z_4A_1K_1C_1F$ are roughly similar, but markedly different from those of the corresponding unreduced state; the interfaces seem to be built of "slats" between which there are many cracks and channels. Obviously, $Z_4A_2K_1C_1F$ has more pores than $Z_4A_1K_1C_1F$. We believe that since Al_2O_3 is a textural promoter, a higher concentration of Al_2O_3 in the catalyst produces more pores.

We also observe small grains in cracks and channels, which are remarkly different from the "slats." In order to detect ZrO_2,

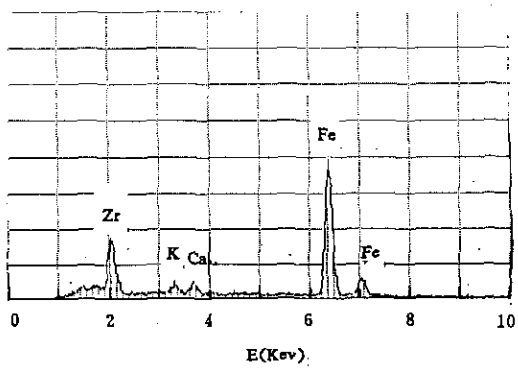

FIG. 8. Energy dispersion X-ray spectrum of the reduced $Z_4A_2K_1C_1F$ (point 1).

we have carried out an elemental analysis for point 1 (grains) and point 2 (slats) of Figs. 6a and b (the results are shown in Fig. 7 and Fig. 8). Focused EDX measurements indicate that greater amounts of promoters, ZrO_2 and CaO are concentrated on the small grains, i.e., ZrO_2 and CaO mainly exist in the channels and cracks of the reduced catalysts. Previously, we have concluded that the ZrO_2 exists in the form of $Ca_xZr_{1-x}O_{2-x}$ (CaF_2 type) in the fused iron catalyst containing a small amount of CaO. Thus we believe that $Ca_xZr_{1-x}O_{2-x}$ is randomly concentrates in the channels of the reduced catalyst. This suggests that $Ca_xZr_{1-x}O_{2-x}$ is formed out of the α-Fe phase to form a separate phase. On the contrary, no separate $Ca_xZr_{1-x}O_{2-x}$ is present in the corresponding unreduced catalyst. This may be attributed to the technique of catalyst preparation. In the process of the catalyst preparation, the evenly molten mass is suddenly cooled by water, and the molten mixture quickly solidifies. Because of the quick solidification, promoters such as ZrO_2, CaO, Al_2O_3, and K_2O are evenly "frozen" into the catalyst particles and have a more homogeneous distribution. After slow reduction of the catalyst, due to the fact that CaO tends to segregate strongly on surface and because of the nonuniform distribution

TABLE IV

SPECIFIC SURFACE AREA OF CATALYSTS

Sample	BET surface area (m^2/g)	Promoter content (wt%)				Fe^{2+}/Fe^{3+}
		ZrO_2	CaO	Al_2O_3	K_2O	
$Z_{1.5}A_2K_1F$	11.59	1.5	0	2	1	0.44
$Z_{2.5}A_2K_1F$	10.58	2.5	0	2	1	0.47
$Z_{3.5}A_2K_1F$	10.10	3.5	0	2	1	0.46
$Z_4A_2K_1F$	9.50	4	0	2	1	0.44
$Z_4A_2K_1C_1F$	10.10	4	1	2	1	0.53
$Z_{2.5}A_1K_1F$	6.37	2.5	0	1	1	0.45

TABLE V

REDUCTION CHARACTERISTICS OF Z_4F, $Z_{11}F$, AND Z_4C_1F

Sample	Temp. (°C) at initial reduction	Max. rate of reduction ($\% \cdot h^{-1}$)	Temp. (°C) at max. rate	Temp. (°C) at the degree of reduction α				
				0.2	0.4	0.6	0.8	0.95
$Z_{11}F$	376	7.87	476	438	453	463	483	497
Z_4C_1F	363	7.94	488	437	465	478	496	513
Z_4F	395	6.81	511	476	500	522	528	531

(*19*), the particles of $Ca_xZr_{1-x}O_{2-x}$ redistribute and combine with each other to form a separate phase existing in the channels of the reduced catalyst.

From Fig. 6c, we can note that the interface of $Z_4A_2K_1F$ (without CaO) is more regular, seems to be built of small rocks or bricks, and that there are fewer channels and pores. However, because of the limitations of measurement resolution, some pores may not show up. The EDX measurement indicates that ZrO_2 distributes evenly in the catalyst. Previously, we have mentioned that Fe^{2+} may enter the ZrO_2 lattice to form a solid solution, $Fe_x^{2+}Zr_{1-x}O_{2-x}$ ($x < 1$). Therefore, because of the formation of $Fe_xZr_{1-x}O_{2-x}$, ZrO_2 is relatively homogeneously distributed both in the unreduced and in the reduced catalyst.

3. Specific Surface Area.

BET surface areas of catalyst samples are listed in Table IV. The specific surface area of the catalyst decreases with the contents of ZrO_2 increase, but the change is not very great (from 11.59 to 9.50 m^2/g). Table IV also suggests that Al_2O_3 is a good textural promoter and that CaO seems to have no influence on the specific surface area of the catalyst.

4. Reduction Behavior

Table V indicate that samples $Z_{11}F$ and Z_4C_1F are more easily reduced than Z_4F. This verifies that ZrO_2 promotes the reduction of iron oxides. Interestingly, CaO itself has no remarkable effect on the reduction of fused iron catalysts, but the experiment indicates that the reduction of Z_4C_1F is much easier than that of Z_4F.

Acknowledgment

We gratefully acknowledge the support of this work by the National Nature Science Foundation Committee of the People's Republic of China.

References

1. W. B. Blumenthal, "The Chemical Behavior of Zirconium," p. 174, Van Nostrand, New Jersey (1958).
2. M. Ichikawa, *Chemtech* **12,** 674 (1982).
3. C. D. Chang and P. D. Perkins, U.S. Patent 4,440,668 (1984).
4. D. Gasser and A. Baker, *Appl. Catal.* **48**(2), 279 (1989).
5. T. Inoue, T. Lizuka, and K. Tanabe, *Bull. Chem. Soc. Jpn.* **60,** 2663 (1987).
6. Q. Zhang, Z. Xu, and Z.-H. Qian, *J. Catal. (China)* **10**(1), 22 (1989).
7. P. H. Emmett, "Catalysis," Vol. 4, p. 146, Reinhold, New York, 1956.
8. Iu. B. Kagan, A. N. Bashkirov, L. I. Zvezdkina, and N. A. Orlova, "Works of Petroleum Institute, Academy of Sciences, USSR," Vol. XII, pp. 200–212 (1958).
9. Xu Jie, "Studies on The Catalysts of Alcohols Synthesis from CO/H_2," Master's Thesis, Zhengzhou University (1988).
10. N. B. Jackson and J. G. Ekerdt, *J. Catal.* **101,** 90 (1986).
11. R. G. Silver, C. J. Hou, and J. G. Ekerdt, *J. Catal.* **118,** 400 (1989).
12. W. C. Maskell and B. C. H. Stelle, *J. Appl. Electrochem.* **16,** 475 (1986).
13. C.-S. Zhang and W.-X. Wang, *J. Catal. (China)* **8**(2), 145 (1987).
14. See Ref. (*1*), p. 161.
15. C.-S. Zhang and W.-X. Wang, *Acta Chim. Sinica* **44,** 1172 (1986).
16. F. Li, W.-X. Wang, Q.-K. Han, and L. Wang, *J. Solid State Chem.* **87**(2), 264 (1990).
17. See Ref. (*1*), pp. 166, 167, and 197.
18. Z. Liu, W.-X. Wang, and F. Li, *J. Zhengzhou Univ.* **1,** 10 (1991).
19. W.-X. Wang and C.-S. Zhang, *in* "Third China–Japan–U.S.A. Symp. Catal., Xiamen, China, August, 1987," p. 113.
20. A. R. West, "Solid State Chemistry and its Applications," p. 478, Wiley, New York (1984).